Analysis of Ultra-Broadband Amplified Spontaneous Emissions Generated by Cr^{4+}:YAG Single and Glass-Clad Crystal Fibers

Kuang-Yao Huang, Kuang-Yu Hsu, and Sheng-Lung Huang, *Senior Member, IEEE, Member, OSA*

***Abstract*—Numerical analysis and experimental verification of the ultra-broadband amplified spontaneous emissions (ASEs) generated by Cr^{4+}:YAG crystal fibers are presented. Milliwatt ASE was obtained from a double-clad 25-μm-core fiber. Results of the experimental ASE power measurements and the composition analysis using electron probe micro-analyzer were used to determine the absorption, emission, and excited-state absorption cross sections of pump and signal of the crystal fibers. The numerical analysis showed that the ASE output power is improved by reducing the fiber core diameter down to several micrometers despite of the increased consumption in excited-state absorption of pump. A comparison of the cross sections between those in literature and this work indicates that the crystal fiber has good crystal and optical qualities using the laser heated pedestal growth method. The large pump absorption of the Cr^{4+}:YAG crystal fiber limits its useful length. With such short fiber length, the ASE lights can not acquire enough gain. The ASE efficiency can be further improved by using bi-direction and cladding pump structure to increase the crystal fiber length and incorporating a high ASE reflector at the input end of the crystal fiber. The Cr^{4+}:YAG crystal fiber has a potential for applying to ultra-broadband ASE light source in wavelength division multiplexing network.**

***Index Terms*—Amplified spontaneous emission, codrawing laser heated pedestal growth, Cr^{4+}, double-clad, fiber amplifier, YAG.**

I. Introduction

DUE TO THE FAST growing communication need, the required capacity of the optical fiber network has been more than doubled every year and the technology break through in dry fiber fabrication opens the possibility for fiber bandwidth all the way from 1.3 to 1.6 μm. The fast increasing demand of communication capacity results in the emergence of wavelength division multiplexing (WDM) technology, enabling tens or even hundreds of channels with different wavelengths transmitted simultaneously on an optical fiber [1].

In consequence, it necessitates the requirement of broadband spectral characteristics of all the optical components used in the optical network systems.

Manuscript received October 27, 2007; revised January 23, 2008. This work was supported in part by the National Science Council, R. O. C.

K.-Y. Huang is with the Institute of Electro-Optical Engineering, National Sun Yat-Sen University, Kaohsiung, Taiwan 804, R.O.C. (e-mail: m9035606@student.nsysu.edu.tw).

K.-Y. Hsu and S.-L. Huang are with the Graduate Institute of Photonics and Optoelectronics, National Taiwan University, Taipei, Taiwan 106, R.O.C. (e-mail: kuangyuhsu@seed.net.tw; slhuang@cc.ee.ntu.edu.tw).

Color versions of one or more of the figures in this paper are available online at http://ieeexplore.ieee.org.

Digital Object Identifier 10.1109/JLT.2008.919448

Broadband light source is one of the key components in WDM networks. Rare earth elements doped silicate fibers are the most common optical fiber light sources. They are highly efficient and mature techniques already [2]–[9]. Transition metal doped garnet crystals are attractive gain media because of their ultra-broadband emission spectra. The active electrons of transition metal ions are not completely shelled by the electron cloud. The subtle interplay between the Coulomb fields of the host matrix ions and the electron-phonon coupling permit ultra-broad absorption and emission spectra. Among the transition metals, Chromium ion is most suitable for doping into the garnet crystal due to its chemical stability, broad absorption bands and large energy-level splitting. The optical characteristics of various Cr^{4+} ion doped hosts are listed in Table I [10]–[12]. The 3-dB emission bandwidth of Cr^{4+}:YAG is 277 nm that covers the widest wavelength range in the communication bands. As shown in Table I, Cr^{4+}:YAG has the largest $\Delta\lambda\sigma_e\tau_f$ product; therefore, Cr^{4+}:YAG has a potential for a broadband light source in the future WDM networks.

In this paper, complete analysis of the broadband amplified spontaneous emissions (ASEs) generated by Cr^{4+}:YAG crystal fibers are presented. The simulations indicate that the ASE efficiency is impacted by the fiber core diameter and the propagation loss. The analyses were verified by the ASE experiments using a codrawing laser heated pedestal growth (CDLHPG) technique for preparing samples with several core diameters [13], [14]. By reducing the core diameter from 920 to 25 μm, the brightness of the generated ASE was increased by a factor of 6.8×10^4. The emission cross section that fitted with the experiments was 7×10^{-19} cm^2, it was larger than the average in literature. The results show that the CDLHPG technique is able to fabricate high quality Cr^{4+}:YAG crystal fibers. The simulation results also show that by reducing the core-diameter down to few-micrometer with the 4.5-cm^{-1} absorption coefficient, tens-milliwatt ASE output can be achieved. A comparison between the parameters of Chromium-doped fiber (CDF) and Erbium-doped fiber (EDF) is given.

II. Numerical Model

The energy level diagram of the Cr^{4+}:YAG crystal is shown in Fig. 1 [15]–[17]. It is basically a four-level system. The Cr^{4+} ions at ground state $^3A_2$ are excited to the $^3T_2$ state by the pumping light. The ions then relax non-radiatively to the meta-stable state $^3B_2\left(^3T_2\right)$. When the electrons translate from $^3B_2\left(^3T_2\right)$ to $^3B_1\left(^3A_2\right)$, photons are generates by stimulated

TABLE I
LIST OF THE Cr^{4+}-ION DOPED HOSTS WITH THE 3-dB EMISSION BANDWIDTH $\Delta\lambda$, PEAK WAVELENGTH, EMISSION CROSS SECTION σ_e, FLUORESCENCE LIFETIME τ_f, AND $\Delta\lambda\sigma_e\tau_f$ PRODUCT AT ROOM TEMPERATURE

Host	Emission spectra (nm)	Peak wavelength (nm)	Emission bandwidth (nm)	σ_e (10^{-19} cm^2)	τ_f (μs)	$\Delta\lambda\sigma_e\tau_f$ (10^{-17} nm·μs·cm^2)
Y_2SiO_5	1162-1416	1260	254	—	0.7	—
Forsterite	1167-1345	1244	178	1.4	3.9	9.7
LAG	1254-1486	1370	232	3.4	5.6	44.2
YAG	1253-1530	1380	277	7.0	4.5	87.3
YSAG	1289-1525	1407	236	3.3	3.3	25.7
GGG	1327-1557	1442	230	4.5	2.2	22.8
YGG	1337-1575	1456	238	4.3	1.9	19.5
YSGG	1421-1701	1561	280	5.2	1.3	18.9
GSGG	1432-1732	1582	300	3.6	2.0	21.6
GSAG	1461-1737	1599	276	4.8	1.7	22.6

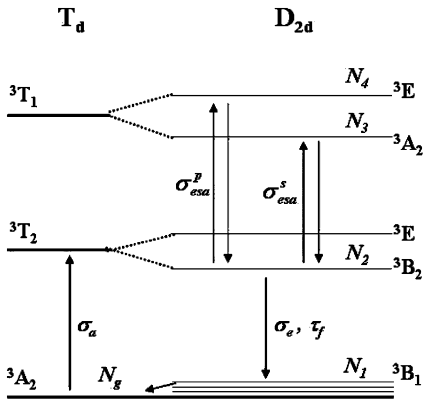

Fig. 1. Energy-level diagram of Cr^{4+}:YAG.

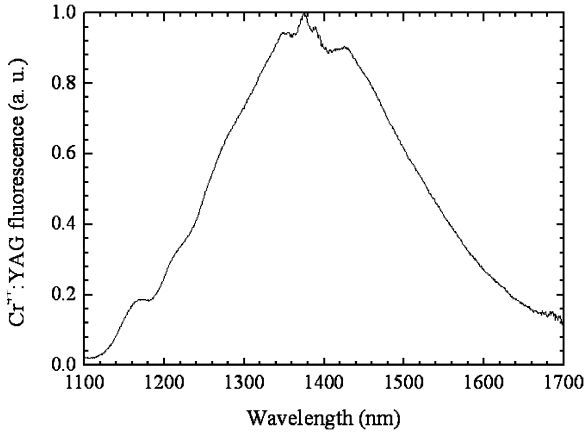

Fig. 2. Cr^{4+}:YAG spontaneous emission spectrum.

and spontaneous emissions. The broadband spontaneous emission spectrum covers from 1.2 to 1.6 μm as shown in Fig. 2. The definitions of N_g, N_1, N_2, N_3, and N_4, are the population densities of ${}^3A_2$, ${}^3B_1\left({}^3A_2\right)$, ${}^3B_2\left({}^3T_2\right)$, ${}^3A_2\left({}^3T_1\right)$, and ${}^3E\left({}^3T_1\right)$, respectively. The Cr^{4+} ions at ${}^3B_2\left({}^3T_2\right)$ not only involve the spontaneous and stimulated emissions to the lower state ${}^3B_1\left({}^3A_2\right)$, also the excited-state absorptions (ESAs) of the ASE and pump to a higher state ${}^3A_2\left({}^3T_1\right)$ and ${}^3E\left({}^3T_1\right)$. The N_1, N_3, and N_4 are assumed to be negligible due to the fast non-radiative relaxation rates. The N_1 is relaxed to ground state ${}^3A_2$; both the N_3 and N_4 are relaxed to meta-stable state ${}^3B_2\left({}^3T_2\right)$. The rate equation for the $N_2(z)$ is given by

$$\frac{dN_2(z)}{dt} = \frac{\sigma_a I_p(z)}{h\nu_p} N_g(z) - N_2(z) \times \left[\sum_i \frac{\sigma_e(\nu_i) I_{ASE}(z,\nu_i)}{h\nu_i} + \frac{1}{\tau_f}\right] \quad (1)$$

$$N_o = N_g(z) + N_2(z) \quad (2)$$

where σ_a is the absorption cross section at pumping frequency ν_p, $\sigma_e(\nu_i)$ is the stimulated emission cross section at emission frequency ν_i, $I_p(z)$ is the pumping intensity, $I_{\mathrm{ASE}}(z)$ is the total ASE intensity including both the forward and backward ASEs, τ_f is the fluorescence lifetime, and h is Planck's constant. The total ion density N_o is equal to the sum of the $N_g(z)$ and $N_2(z)$ since the population densities in all other energy states are assumed to be negligible. From (1) and (2), the steady-state solution of the population density $N_2(z)$ can be expressed as

$$N_2(z) = N_0 \cdot \frac{\frac{\sigma_a I_p(z)}{h\nu_p}}{\frac{\sigma_a I_p(z)}{h\nu_p} + \sum_i \frac{\sigma_e(\nu_i) I_{ASE}(z,\nu_i)}{h\nu_i} + \frac{1}{\tau_f}}. \quad (3)$$

By assuming uniform light intensity across the fiber cross section for $I_p(z)$ and $I_{\mathrm{ASE}}(z)$, the transport equations for the pumping and ASE intensities can be expressed as

$$\frac{dI_p(z)}{dz} = -\left[\sigma_a \cdot N_g(z) + \sigma_{\mathrm{esa}}^p \cdot N_2(z) + \alpha_{pl}^p\right] \times I_p(z) \quad (4)$$

$$\frac{dI_{\mathrm{ASE}}^{\pm}(z,\nu_i)}{dz} = \pm\sigma_e(\nu_i) N_2(z) \times \left\{\left[1 - \frac{\sigma_{\mathrm{esa}}^s(\nu_i)}{\sigma_e(\nu_i)}\right] \times I_{\mathrm{ASE}}^{\pm}(z,\nu_i) + M \times 2h\nu_i\Delta\nu_i\right\} \mp \alpha_{pl}^{\mathrm{ASE}} \times I_{\mathrm{ASE}}^{\pm}(z,\nu_i) \quad (5)$$

where α_{pl}^p and $\alpha_{pl}^{\mathrm{ASE}}$ are the propagation loss constants of the pump and ASE, respectively, and are the ESA cross section of pump and ASE, respectively, σ_{esa}^p is the emission frequency, σ_{esa}^s is the mode number of ASE [18], and $\Delta\nu_i$ is the divided bandwidth of the emission spectrum [19]–[21]. The positive and negative signs in (5) represent the forward and backward propagating ASEs, respectively. The Cr^{4+} ions within a differential fiber length dz contribute to the generation of the spontaneous emission and also the amplification of the forward and backward ASEs.

The computation results indicate that the core-diameter of fiber is a critical factor to the ASE output power. Reduction of the core-diameter can increase the pumping and signal light intensity to obtain higher ASE output power and reduce the number of guiding mode.

III. Sample Preparation and ASE Measurements

A. Sample Preparation

In order to verify the effect of the core-diameter on the ASE output power, fibers with several core-diameters were prepared. The laser heated pedestal growth (LHPG) method was used for the growth of the Cr:YAG crystal fiber [22]. The absorption coefficient of the Cr:YAG source crystal rod was 4.5 cm^{-1} at 1064-nm wavelength. The Cr_2O_3 doping concentration was 0.25 wt.% in the source rod measured by electron probe microanalyzer (EPMA). Single crystalline 920- and 100-μm diameter fibers were sequentially grown in the $\langle 111 \rangle$ orientation. However, for the growth of fiber with its diameter less than 30μm, it becomes very difficult. It is limited by the power stability of the CO_2 laser. The CDLHPG technique provides a solution to further reduce the core diameter of the fiber. In this way, the resultant core diameter could be reduced to less than 30 μm. First, a 68-μm diameter Cr:YAG crystal fiber was obtained by a two-step growth from a 500-μm diameter source rod. Then it was inserted into a fused-silica capillary tube with 76- and 320-μm inner and outer diameters. The 1970 °C melting temperature of the YAG is comparable to the 1600 °C soften temperature of the fused-silica. The heating of the CDLHPG method caused a strong inter-diffusion between the YAG core and fused-silica capillary, and an inner cladding layer made of the mixture was formed. With properly controlled growth parameters, double-clad Cr^{4+}:YAG crystal fibers were obtained. The core diameter of the double-clad fiber was controlled during growth process by adjusting the CO_2 laser power and the fiber growth speed.

The composition analysis was done by EPMA. The result showed that the core and outer-clad were almost YAG and SiO_2, respectively. The compositions of the inner-clad were mixtures of YAG and SiO_2. We also used high-resolution transmission electron microscopy (HRTEM) and selected area electron diffraction (SAED) to confirm that the core structure of the double-clad Cr^{4+}:YAG fiber remained crystalline [23]. The Cr^{4+} fluorescence intensity and refractive index profiles on the cross section of the double-clad fiber were measured by a laser scanning optical microscope. As shown in Fig. 3, the Cr^{4+} fluorescence concentrates mainly within the core region. The refractive indices of the core, inner-clad, and outer-clad are 1.82, 1.66, and 1.46, respectively. The uniformity of the core diameter is very sensitive to the heating power by the CO_2 laser. The laser power was maintained with $\pm 0.5\%$ stability by using a motorized polarizer with a feedback control loop for obtaining a 25-μm core double-clad fiber. For fabricating a fiber with core-diameter smaller than 25-μm double-clad crystal fiber, a better control of the heating laser power is required.

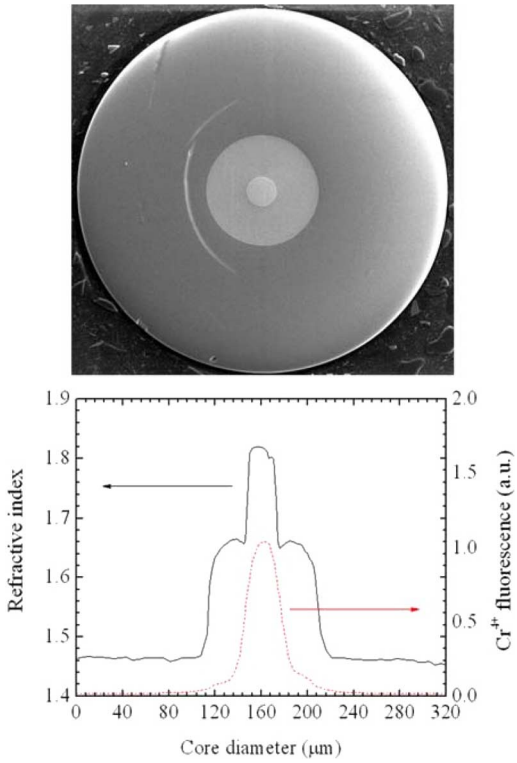

Fig. 3. Image (top) is the end face of the double-clad Cr^{4+}:YAG crystal fiber. The figure (bottom) shows the refractive index and Cr^{4+} fluorescence profiles.

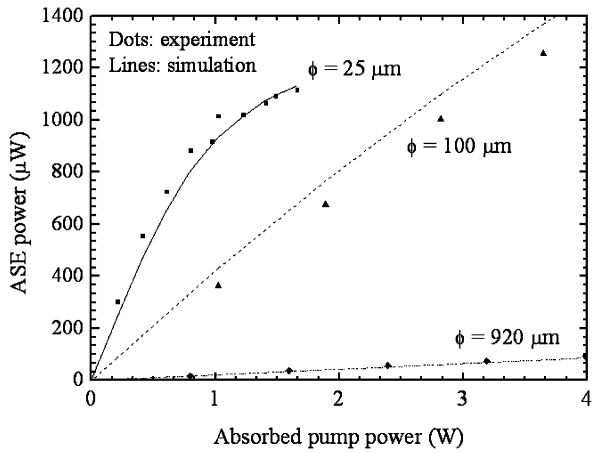

Fig. 4. ASE powers versus pump powers for the samples with core diameters of 920, 100, and 25 μm. The dots and the lines represent the measured and the simulated data.

B. ASE Measurements

A 1064-nm Yb-fiber laser with its wavelength at the peak of the Cr^{4+}:YAG absorption spectrum was used to pump the Cr^{4+}:YAG crystal fibers with 920-, 100-, and 25-μm core diameters. We used the end pumping scheme for the ASE generation. The pump light was launched into the core at one polished end of the crystal fiber. The corresponding fiber lengths were 1.5, 4.7, and 5.5 cm, respectively. Fig. 4 shows the measured and simulated ASE powers as a function of the absorbed pump power. In the experiments, the ASE efficiency of 25-μm core fiber with the strongest optical confinement obtained the higher

TABLE II
SUMMARY OF THE ABSORPTION, EMISSION, AND EXCITED-STATE ABSORPTION OF PUMP AND SIGNAL CROSS SECTIONS OF OUR CRYSTAL FIBER AND SAMPLES DESCRIBED IN THE LITERATURES

Reference	$\sigma_a(\times 10^{-19}$ cm$^2)$	$\sigma^p_{esa}(\times 10^{-19}$ cm$^2)$	σ^p_{esa}/σ_a	$\sigma_e(\times 10^{-19}$ cm$^2)$	$\sigma^s_{esa}(\times 10^{-19}$ cm$^2)$	σ^s_{esa}/σ_e
[12]	—	—	—	3.3	—	—
[13]	11.2	—	—	0.47	0.093	19.8%
[14]	16.5	4.4	26.6%	—	1.2	—
[24]	50	5	10%	8	5	62.5%
[25]	57	8	14%	—	—	—
[26]	30	2	6.7%	—	2	—
[27]	57	—	—	3.5	—	—
[28]	8.7	—	—	2.2	—	—
[29]	25	—	—	—	3	—
[30]	70	20	28.6%	—	—	—
[31]	31	—	—	3.4	1.8	52.9%
[32]	8	—	—	0.95	—	—
Mean	30.4	7.88	17.2%	3.1	2.2	45.1%
This work	22	4.2	19%	7	1.4	20%

efficiency. The roll-off in the $\phi = 25\,\mu$m curve is due to the short CDF length. The ASE power can be further improved by both reducing the core diameter and increasing the fiber length.

IV. DISCUSSION

A. Parameter Fitting

The ratio between the absorption and emission cross sections is critical to the ASE efficiency. Table II shows the absorption, pump ESA, emission, and signal ESA cross sections of our Cr^{4+}:YAG fiber and the samples described in literature. The means of the absorption, pump ESA, emission, and signal ESA cross sections of the crystals described in literature are 30.4×10^{-19} cm^2, 7.88×10^{-19} cm^2, 3.1×10^{-19} cm^2, and 2.2×10^{-19} cm^2, respectively. For our fiber, these parameters derived from curve fitting are 22×10^{-19} cm^2, 4.18×10^{-19} cm^2, 7×10^{-19} cm^2, 1.4×10^{-19} cm^2, respectively. The crystal fiber growth by the LHPG method has large emission cross section compared with the average value in literature while the absorption cross section is slightly lower than the average value. The average pump and signal ESA cross sections of our samples are also lower than the average value. Over all, the fitting result shows that the double-clad crystal fibers have good quality for optical emission.

The numerical aperture of the double-clad 25-μm core fiber is around 0.75 from the refractive index measurement in the Fig. 3. The normalized frequency V-value of such a fiber is 56 at 1.4-μm wavelength. By the curve fitting, the ASE mode numbers were 5, 28, and 120 in the 25-, 100-, and 920-μm crystal fibers; though the mode estimation should all exceed 1000 modes depended on V-value. It implied that the few modes were generated and guided in the active waveguide.

B. Power Budget of the Pump Laser

The power budget of pump power for the ASE experiment of the 25-μm core fiber was calculated by the simulation. Table III shows the simulated power budget of one-watt absorbed pump power to the propagation losses and ESAs of pump and ASE, quantum defect, nonradiative decay of population, and ASE, respectively. From the simulation of fibers with several core-diameters, the results indicated that the ASE efficiency rises up with the reduced core diameter, although the pump ESA dissipation also increases. The conditions for each case ESA were optimized for the highest ASE output. The absorption coefficient of pump was assumed to be 4.5 cm^{-1}. The mode number of local spontaneous emission was assumed to be one to simplify the uncertain value of mode number. The simulation results were shown in Table III.

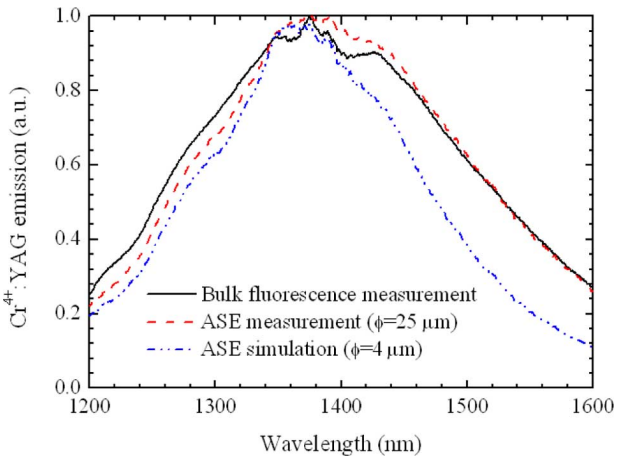

Fig. 5. Cr^{4+}:YAG emission spectra.

When the core diameter was reduced from 25 to 4 μm, the ASE output can be improved around from 0 to 18 dBm. For the 4-μm core case, the major loss is the pump ESA which is doubled that compared to the loss of 25-μm core fiber case. Fig. 5 shows the Cr^{4+}:YAG measured emission spectra of bulk crystal and 25-μm core fiber, and simulated ASE simulation of 4-μm core fiber. The emission bandwidths were 277, 265, and 205 nm, respectively. As the efficiency increase, the ASE spectra width decreases, mostly in the 1.5-μm region.

TABLE III
LIST OF THE POWER BUDGET OF FIBERS WITH SEVERAL CORE DIAMETERS WITH ONE WATT PUMP POWER. THE SECOND COLUMN IS THE NUMERICAL ANALYSIS OF THE ASE EXPERIMENT WITH 25-μm CORE FIBER. THE THIRD AND FOURTH COLUMNS CALCULATE THE REQUIREMENTS TO OBTAIN TENS-MILLIWATT ASE OUTPUT

	Simulation of 25-μm core fiber	Simulation of 8-μm core fiber	Simulation of 4-μm core fiber
Power budget	Percentage (%)	Percentage (%)	Percentage (%)
Propagation loss of pump	15.5	3.71	4.3
Pump ESA	35.4	62.4	76
Quantum defect	11.4	8	4.5
Non-radiative decay of population	37.51	23.5	7.55
Propagation loss of ASE	0.006	0.04	0.12
ASE ESA	0.008	0.44	1.5
ASE 4π radiative loss	0.084	0.11	0.13
ASE	0.092	1.8	5.9
Total absorbed pump power	100	100	100

C. Absorption Coefficient

The doping distributions on the cross sections of the crystal fibers were measured by the EPMA. From the measurement results with several growth conditions, it was observed that the Cr ion concentration decreased after each growth. The decrease is due to Cr ions out diffusion and evaporation at the perimeter of the fiber during growth. The average concentration of CaO, acting as Cr^{4+} charge compensators, only slightly decreased by less than 10%. But the average Cr_2O_3 concentration decreased quickly during the fiber diameter reduction process. The average Cr_2O_3 concentration during the size reduction process of the crystal fiber is shown in Fig. 6. An empirical formula for the average Cr_2O_3 concentration was derived as

$$C_{Cr_2O_3} = 0.68 C_0 \left(\frac{s}{\gamma}\right)^{1/2} D^{1/3}, \text{ when } \frac{s}{\gamma} \le 1.7 \quad (6)$$

where C_0 is the average Cr_2O_3 concentration of the source rod material, s and γ are the growth speed and pull/push speed ratio, respectively. D is the diameter of source rod.

Crystal fiber grown from a source rod with a larger diameter and at a faster speed will have higher Cr concentration because it takes longer time for the Cr ions to diffuse from the molten zone center to the circumference. For the case of the 25-μm core fiber, the Cr_2O_3 concentration was reduced from 0.25 wt.% to 0.04 wt.% with two diameter reduction steps. The absorption coefficient reduced significantly from 4.5 cm^{-1} to 0.7 cm^{-1}. Although the absorption coefficient is reduced, it is still rather large from the fiber amplifier's point of view. For constructing an efficient fiber ASE light source, a longer length of CDF is desired so the spontaneous emission captured by the fiber can be sufficiently amplified as it propagates along the gain fiber in either forward or backward direction. However, the pump absorption along the fiber is large due to the relatively large ground state absorption and the ESA of the pump. To replenish the Cr ions can further reduce the required CDF length for ASE light source. The circumferential surface of the source rod can be deposited with the Cr_2O_3 thin layer after the first growth step, the Cr ions then diffuses into the 68-μm core fiber in the second growth step.

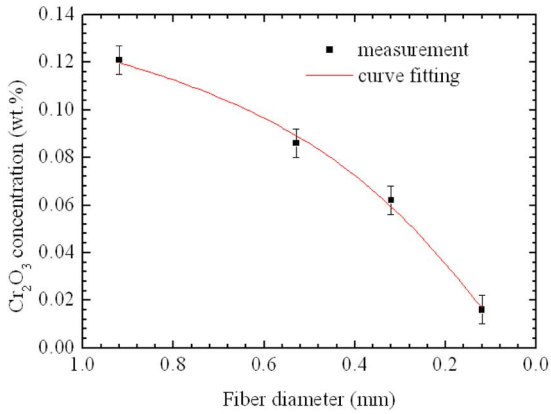

Fig. 6. Average Cr_2O_3 concentrations of various fiber diameters.

D. Propagation Loss

By using the cut-back method, the propagation losses of the single crystal fiber and double-clad crystal fiber were found to be 0.6 dB/cm and less than 0.2 dB/cm at the wavelength of 1064 nm. The propagation loss of the double-clad crystal fiber is less than that of the single crystal fiber. The major reason is due to the strong inter-diffusion between the fused-silica and YAG during the CDLHPG process for fabricating the double-clad fiber. It has a smooth and clear interface between the core and the inner-clad, so the scattering of the interface defects can be reduced. Also the core diameter and the refractive index difference between core (1.82) and cladding (1.66) were reduced.

TABLE IV
PARAMETERS OF THE CDF AND A TYPICAL ERBIUM DOPED FIBER, WHERE THE σ_a^s IS THE ABSORPTION CROSS SECTION FOR EMISSION WAVELENGTH. THE v_s IS ASSUMED TO BE THE 1400-nm CENTER EMISSION WAVELENGTH FOR CALCULATING $I_s^{\rm sat}$

Parameter	CDF	EDF	Unit
N_T	3.2×10^{17}	80×10^{17}	cm^{-3}
σ_a	22×10^{-19}	0.025×10^{-19} @ 980 nm 0.018×10^{-19} @ 1480 nm	cm^2
σ_e	7×10^{-19}	0.050×10^{-19} @ 1552 nm	cm^2
σ_e/σ_a	0.318	2 @ 980n nm pump 2.78 @ 1480 nm pump	
σ_{esa}^p	4.2×10^{-19}	—	cm^2
σ_{esa}^s	1.4×10^{-19}	—	cm^2
σ_a^s	—	0.023×10^{-19} @ 1552 nm	cm^2
τ_f	4.5	~10000	μs
$\Delta\lambda$	265	30	nm
I_p^{sat}	18.8×10^3	8.1×10^3 @ 980 nm 7.5×10^3 @ 1480 nm	W/cm^2
I_s^{sat}	45×10^3	2.56×10^3	W/cm^2

During the fiber growth, the temperature gradient between the interface of the solid and the melt is as high as 1×10^3 °C/cm; therefore, residual strain exists in the interface between core and inner-clad of the double-clad fiber. To release the residual strain and further reduce the propagation loss of the double-clad fiber, post-growth annealing is suitable.

E. Comparison Between CDF and EDF

The important optical parameters of the CDF and a typical EDF are summarized in Table IV [33]. The active ion concentration of a typical EDF is much higher than the CDF's. This is because the Erbium ions in the silica host are naturally in the desired trivalent state. The highest Erbium doping concentration is limited by the interactions between the Erbium ions like up-conversion and concentration quenching. Unlike the EDF case, the Chromium ions in the YAG host are initially in the trivalent state. A charge compensation mechanism is used to turn the oxidation state of some of the Chromium ions into the quadrivalent state. The charge compensation efficiency for generating Cr^{4+} ions out of the Cr^{3+} ions is typically less than 6%. Most of the Chromium ions still remain in the trivalent state. This charge compensation efficiency is the limiting factor of the Cr^{4+} concentration. As described in the previous section, the Chromium ions evaporate out of the melt during the fiber growth process so the Cr^{4+} concentration of the fiber further decreases.

The pump absorption cross section and the signal stimulated emission cross section of the CDF are several orders of magnitude larger than those of the EDF. As shown in (4) and (5), the absorption constant and the gain constant are related to the products of the Cr^{4+} ion concentration and the corresponding cross sections. These products $\sigma_a N_o$ and $\sigma_e N_o$ of the CDF are 35 and 5 times larger than those of the EDF. This implies required CDF length will be shorter, which is favorable with consideration of the significant propagation losses of the CDF. The CDF length could be even shorter by increasing the Cr^{4+} doping concentration. The $\sigma_e N_o$ product related to the gain constant of the CDF is absolutely large as compared to that of the EDF. However, for the application of fiber ASE light source, the relative magnitude of $\sigma_e N_o$ compared to its own $\sigma_a N_o$ product is more suitable for evaluation of its performance. The $\sigma_e N_o$ product of the CDF is about one third of its $\sigma_a N_o$ product. If including the effect of the ESAs of the pump and ASE, the ratio of the ASE gain constant to the pump absorption constant becomes even smaller. As a result, before the ASEs acquire sufficient gain the pump light in CDF already decays below its pump saturation intensity and has no ability to achieve population inversion within a short fiber length. Using the EDF as a reference, its $\sigma_e N_o$ product is two times of the $\sigma_a N_o$ product for 980-nm pump. Therefore the ASE can acquire enough gain while it propagates along the gain fiber. The σ_e/σ_a ratio is a useful parameter in evaluating an optical material for a fiber ASE source or amplifier. Although the wide emission bandwidth is very attractive, the light amplification ability of the Cr^{4+}:YAG is not so strong as its σ_e/σ_a ratio is only 0.318. For EDF, the σ_e/σ_a ratios are 2 and 2.78 for 980- and 1480-nm pumps, respectively. Measures to further improve the ASE efficiency of CDF are necessary. In order to extent the CDF length that the pump light can deliver its power along and thus improve the ASE powers, the bi-directional pumping scheme is suitable. In addition, since our CDF has a double-cladding structure, cladding pump scheme is useful in relieving the pump absorption while keeping the same gain constant since both the forward and backward ASEs are only propagating in the core. Incorporating a high reflectivity mirror at the input end of the CDF will improve the ASE efficiency because the backward ASE is reflected and can experience more gain as it travels again through the CDF.

The lifetime of the CDF is about three orders of magnitude shorter than that of the EDF. The pump power for EDF can be as low as a few tens of milliwatts but still maintaining a good optical efficiency due to the long lifetime of the Erbium ion. For CDF the much shorter lifetime of the excited Cr^{4+} ions leads to a faster spontaneous emission rate. As a consequence, a faster pumping rate is required for the CDF for maintaining the excited state population. The saturation intensities described below are useful in evaluating the optical materials as gain media

$$I_p^{\rm sat} = \frac{h\nu_p}{\sigma_e \tau_f} \tag{7}$$

$$I_s^{\rm sat} = \frac{h\nu_s}{\sigma_e \tau_f} \tag{8}$$

where $I_p^{\rm sat}$ and $I_s^{\rm sat}$ are the saturation intensities of the pump and ASE, ν_s is the emission frequency. As shown in Table IV, the pump saturation intensity of the CDF is about two times larger than that of the EDF. The much larger cross-sections of CDF compensate the drawback of its short lifetime. So the much shorter lifetime of the CDF does not cause a serious issue in

achieving population inversion. But when taking into consideration that the core diameter of the CDF is much larger than the EDF's, which can be as small as 3–4 μm, the pump power of CDF will be much larger. In our calculation, the pump power for the CDF should be at least in the order of watt level to have a better ASE output power. The low ASE efficiency of the CDF can be ascribed to the relatively small emission cross-section, compared with its own pump absorption cross-section.

V. Conclusion

A complete numerical model was established for investigating the ASE efficiency of the Cr^{4+}:YAG crystal fibers. The numerical results shows that the ASE efficiency is significantly influenced by the core diameter of the Cr^{4+}:YAG crystal fibers. But it also tormented by the pump ESA with the reduction process of the core diameter. As the simulations, the ASE power could be improved from 0 dBm to 18 dBm for a 4-μm core fiber with an absorption coefficient of 4.5 cm^{-1} in one watt pump. In our experiments, the ASE efficiency of a 25-μm core double-clad fiber was demonstrated to have improvements compared with those of the 920- and 100-μm core single crystal fibers. By curve fitting of the ASE experiments for the absorption, emission, and ESA of pump and signal cross sections, they were found to be 22×10^{-19} cm^2, 7×10^{-19} cm^2, 4.2×10^{-19} cm^2, and 1.3×10^{-19} cm^2, respectively. Compared with those in literature, the crystal fibers grown by LHPG method are good in optical performance and crystal quality. The present low ASE efficiency of the CDF is ascribed to the relatively low emission cross-section and the large ground-state and excited-state absorption cross sections of the pump. The ASE efficiency can be further improved by using bi-directional and cladding pump structure to extend the CDF length and increase ASE gain and incorporating a high ASE reflector at the input end of CDF to redirect the backward ASE.

References

[1] T. Ono and Y. Yano, "Key technologies for terabit/second WDM systems with high spectral efficiency of over 1 bit/s/Hz," *IEEE J. Quantum Electron.*, vol. 34, no. 11, pp. 2080–2088, Nov. 1998.

[2] R. J. Mears, L. Reekie, I. M. Jauncey, and D. N. Payne, "Low-noise erbium-doped fiber amplifier operating at 1.54 mm," *Electron. Lett.*, vol. 23, pp. 1026–1027, 1987.

[3] J. F. Massicott, J. R. Armitage, R. Wyatt, B. J. Ainslie, and S. P. Craig-Ryan, "High gain, broadband, 1.6-mm Er^{3+} doped silica fiber amplifier," *Electron. Lett.*, vol. 26, pp. 1645–1646, 1990.

[4] C. A. Millar and P. W. France, "Diode-laser pumped erbium-doped fluorozirconate fiber amplifier for the 1530 nm communications window," *Electron. Lett.*, vol. 26, pp. 634–635, 1990.

[5] Y. Ohishi, A. Mori, M. Yamada, H. Ono, Y. Nishida, and K. Oikawa, "Gain characteristics of tellurite-based erbium-doped fiber amplifiers for 1.5-mm broadband amplification," *Opt. Lett.*, vol. 23, pp. 274–276, 1998.

[6] T. Komukai, T. Yamamoto, T. Sugawa, and Y. Miyajima, "1.47 mm band Tm^{3+} doped fluoride fiber amplifier using a 1.064 mm upconversion pumping scheme," *Electron. Lett.*, vol. 29, pp. 110–111, 1993.

[7] A. Cucinotta, F. Poli, and S. Selleri, "Gain characteristics of thulium-doped tellurite fiber amplifiers by dual-wavelength (800 nm + 1064 nm) pumping," in *Proc. Opt. Fiber Commun. Conf.*, 2003, vol. 2, pp. 625–627.

[8] E. R. M. Taylor, L. N. Ng, J. Nilsson, R. Caponi, A. Pagano, M. Potenza, and B. Sordo, "Thulium-doped tellurite fiber amplifier," *IEEE Photon. Technol. Lett.*, vol. 16, no. 3, pp. 777–779, Mar. 2004.

[9] Y. Ohishi, T. Kanamori, T. Kitagawa, S. Takahashi, E. Snitzer, and G. H. Sigel, Jr, "Pr^{3+}-doped fluoride fiber amplifier operating at 1.31 mm," *Opt. Lett.*, vol. 16, pp. 1747–1749, 1991.

[10] S. Kuck, J. Koetke, K. Petermann, U. Pohlmann, and G. Huber, "Spectroscopic and laser studies of Cr^{4+}:YAG and Cr^{4+}:Y_2SiO_5," *OSA Proc. Adv. Solid-State Lasers*, vol. 15, pp. 334–338, 1993.

[11] W. Koechner, *Solid-State Laser Engineering*. Berlin, Germany: Springer-Verlag, 1996, pp. 66–70.

[12] S. Kuck, K. Petermann, U. Pohlmann, and G. Huber, "Near-infrared emission of Cr^{4+}-doped garnets: Lifetimes, quantum efficiencies, and emission cross sections," *Phys. Rev. B*, vol. 51, pp. 323–331, 1995.

[13] C. Y. Lo, K. Y. Huang, J. C. Chen, S. Y. Tu, and S. L. Huang, "Glass-clad Cr^{4+}:YAG crystal fiber for the generation of super wideband amplified spontaneous emission," *Opt. Lett.*, vol. 29, pp. 439–441, 2004.

[14] C. Y. Lo, K. Y. Huang, J. C. Chen, C. Y. Chuang, C. C. Lai, S. L. Huang, Y. S. Lin, and P. S. Yeh, "Double-clad Cr^{4+}:YAG crystal fiber amplifier," *Opt. Lett.*, vol. 30, pp. 129–131, 2005.

[15] A. Sennaroglu, "Broadly tunable Cr^{4+}-doped solid-state lasers in the near infrared and visible," *Progr. Quantum Electron.*, vol. 26, pp. 287–352, 2002.

[16] G. Xiao, J. H. Lim, S. Yang, E. V. Stryland, M. Bass, and L. Weichman, "Z-scan measurement of the ground and excited state absorption cross sections of Cr^{4+} in yttrium aluminum garnet," *IEEE J. Quantum Electron.*, vol. 35, no. 7, pp. 1086–1091, Jul. 1999.

[17] A. G. Okhrimchuk and A. V. Shestakov, "Absorption saturation mechanism for Yag:Cr^{4+} crystals," *Phys. Rev. B*, vol. 61, pp. 988–995, 2000.

[18] C. E. Chryssou, F. D. Pasquale, and C. W. Pitt, "Improved gain performance in Yb^{3+}-sensitized Er^{3+}-doped alumina (Al_2O_3) channel optical waveguide amplifiers," *IEEE J. Lightw. Technol.*, vol. 19, no. 3, pp. 345–349, Mar. 2001.

[19] P. C. Becker, N. A. Olsson, and J. R. Simpson, *Erbium-Doped Fiber Amplifiers: Fundamentals and Technology*. New York: Academic, 1999, pp. 131–152.

[20] C. Barnard, P. Myslinski, J. Chrostowski, and M. Kavehrad, "Analytical model for rare-Earth-doped fiber amplifiers and lasers," *IEEE J. Quantum Electron*, vol. 30, no. 8, pp. 1817–1830, Aug. 1994.

[21] M. Hofer, M. E. Fermann, A. Galvanauskas, D. Harter, and R. S. Windeler, "Low-noise amplification of high-power pulses in multimode fibers," *IEEE Photon. Technol. Lett.*, vol. 11, no. 6, pp. 650–652, Jun. 1999.

[22] R. S. Feigelson, "Pulling optical fibers," *J. Cryst. Growth*, vol. 79, pp. 669–680, 1986.

[23] Y. S. Lin, C. C. Lai, K. Y. Huang, J. C. Chen, C. Y. Lo, S. L. Huang, T. Y. Chang, J. Y. Ji, and P. Shen, "Nanostructure formation of double-clad Cr^{4+}:YAG crystal fiber grown by co-drawing laser-heated pedestal," *J. Cryst. Growth*, vol. 289, pp. 515–519, 2006.

[24] N. I. Borodin, V. A. Zhitnyuk, A. G. Okhrimchuk, and A. V. Shestakov, "Oscillation of a Cr^{4+} : $Y_3Al_5O_{12}$ laser in wavelength region of 1.34–1.6 mm," *Bull. Acad. Sci. USSR, Phys. Ser.*, vol. 54, pp. 54–60, 1990.

[25] H. Eilers, K. R. Hoffman, W. M. Dennis, S. M. Jacobsen, and W. M. Yen, "Saturation of 1.064 mm absorption in Cr,Ca:$Y_3Al_5O_{12}$ crystals," *Appl. Phys. Lett.*, vol. 61, pp. 2958–2960, 1992.

[26] K. Spariosu, W. Chen, R. Stultz, M. Birnbaum, and A. V. Shestakov, "Dual Q switching and laser action at 1.06 and 1.44 mm in a Nd^{3+}:YAG – Cr^{4+}:YAG oscillator at 300 K," *Opt. Lett.*, vol. 18, pp. 814–816, 1993.

[27] E. Eilers, U. Hommerich, S. M. Jacobsen, and W. M. Yen, "Spectroscopy and dynamics of Cr^{4+}:$Y_3Al_5O_{12}$," *Phys. Rev. B*, vol. 49, pp. 15505–15513, 1994.

[28] Y. Shimony, Z. Burshtein, and Y. Kalisky, "Cr^{4+}:YAG as passive Q-switch and brewster plate in a pulsed Nd:YAG laser," *IEEE J. Quantum Electron.*, vol. 31, no. 10, pp. 1738–1741, Oct. 1995.

[29] S. Camacho-Lopez, R. P. M. Green, G. J. Crofts, and M. J. Damzen, "Intensity-induced birefringence in Cr^{4+}:YAG," *J. Mod. Opt.*, vol. 44, pp. 209–219, 1997.

[30] Z. Burshtein, P. Blau, Y. Kalisky, Y. Shimony, and M. R. Kokta, "Excited-state absorption studies of Cr^{4+} ions in several garnet host crystals," *IEEE J. Quantum Electron.*, vol. 34, no. , pp. 292–299, Feb. 1998.

[31] J. C. Diettrich, I. T. McKinnie, and D. M. Warrington, "The influence of active ion concentration and crystal parameters on pulsed Cr:YAG laser performance," *Opt. Commun.*, vol. 167, pp. 133–140, 1999.

[32] R. Feldman, Y. Shimony, and Z. Burshtein, "Dynamics of chromium ion valence transformations in Cr,Ca:YAG crystals used as laser gain and passive Q-switching media," *Opt. Mater.*, vol. 24, pp. 333–344, 2003.

[33] M. M. Liu, *Principles and Applications of Optical Communications*. Chicago, IL: Irwin, 1996, pp. 877–877.

Kuang-Yao Huang was born in Kaohsiung, Taiwan, in 1978. He received the B.S. degree in electrical engineering from National Sun Yat-Sen University, Taiwan, R.O.C., in 2001, and the M.S. degree from the Institute of Electro-Optical Engineering, National Sun Yat-Sen University, Taiwan, R.O.C., in 2003, where he is currently pursuing the Ph.D. degree.

His research interests include the developments of ultra-broadband amplified spontaneous emission light source, optical amplifier, and fabrication of the crystal fiber with special attention to growth control.

Kuang-Yu Hsu was born in Hualien, Taiwan, R.O.C., in 1968. He received the B.S. and M.S. degrees from National Taiwan University, Taiwan, R.O.C., in 1990 and 1994, respectively, both in electrical engineering. He is currently pursuing the Ph.D. degree at the Graduate Institute of Photonics and Optoelectronics, National Taiwan University.

He has worked in the microwave communication system and the fiber-optics industries for years. His research interests include the design, fabrication, and characterization of the erbium-doped and chromium-doped fiber amplifiers, optical switches, and fiber polarizers.

Sheng-Lung Huang (M'98–SM'04) was born in Taipei, Taiwan, R.O.C., in 1964. He received the B.S. degree from National Taiwan University (NTU), Taiwan, R.O.C., in 1986, and the M.S. and Ph.D. degrees from the University of Maryland, College Park, in 1990 and 1993, respectively, all in electrical engineering.

He is currently a Professor and the Chairman of the Graduate Institute of Photonics and Optoelectronics, NTU. His research interests include laser and nonlinear crystal fiber growth, diode laser pumped solid-state lasers, and dielectric thin-film deposition. He worked for the Institute of Electro-Optical Engineering, National Sun Yat-Sen University, before joining NTU.

Dr. Huang is a member of the Optical Society of America and the Photonics Society of Chinese-Americans. He served as Chairman of IEEE/LEOS Taipei Chapter in 2005–2006, and is presently a Topical Editor of *Optics Letters*.